Optics Letters

# Photoelectron holography and forward scattering in atomic ionization by elliptically polarized laser pulses

Hui Xie,[1] Min Li,[1,*] Siqiang Luo,[1] Yang Li,[1] Jia Tan,[1] Yueming Zhou,[1] Wei Cao,[1] and Peixiang Lu[1,2,3]

[1]Wuhan National Laboratory for Optoelectronics and School of Physics, Huazhong University of Science and Technology, Wuhan 430074, China
[2]Laboratory of Optical Information Technology, Wuhan Institute of Technology, Wuhan 430205, China
[3]e-mail: lupeixiang@hust.edu.cn
*Corresponding author: mli@hust.edu.cn

Received 15 May 2018; revised 6 June 2018; accepted 6 June 2018; posted 7 June 2018 (Doc. ID 331567); published 2 July 2018

**We report on the scaling of the photoelectron holography with the laser ellipticity in strong-field atomic ionization. We find that the spacing of the holographic fringe gradually decreases with increasing of the ellipticity. In terms of the strong-field approximation, the scaling of the fringe spacing with the laser ellipticity is explained by the effect of the initial transverse momenta at the tunnel exit. With increasing of the laser ellipticity, a ridge structure arising from forward scattering electrons is observed in the low-energy region of the electron momentum distribution. An analytic formula is obtained that demarcates the phase diagram for the observation of the holographic pattern and ridge structure in elliptically polarized laser fields.** 

***OCIS codes:*** (020.2649) Strong field laser physics; (260.5210) Photoionization; (320.7120) Ultrafast phenomena.

https://doi.org/10.1364/OL.43.003220

Electrons released from strong-field ionization of atoms and molecules can be either emitted directly (direct electron) or driven back to the parent ion by the oscillating laser field (rescattering electron) [1]. Both direct and rescattering electrons can be used to image the molecular structure and dynamics thus they are very significant in strong-field physics. The recollision electron can further trigger a variety of strong-field phenomena, including high-harmonic generation [2–7], nonsequential double ionization [8–11], and photoelectron diffraction [12,13].

The direct and recollision electron wave packets can lead to a quantum interference effect when their final momenta are the same. This kind of interference is known as strong-field photoelectron holography (SFPH), which was first reported by Huismans *et al.* [14]. In SFPH, the recollision electron acts as a signal wave, while the direct electron acts as a reference wave. The interference of the signal and reference waves in photoelectron momentum distribution (PMD) gives rise to the hologram, i.e., a spider-like interference structure. Bian and Bandrauk predicted the backward scattering photoelectron holography in strong-field ionization of a molecule [15], which was confirmed by subsequent experiments [16]. Because the SFPH has encoded spatial and temporal information for both ions and electrons, it has been used to extract the ion and electron dynamics in atoms and molecules with attosecond and angstrom resolutions [16–21].

It has been explored how the photoelectron holographic structure scales with several laser parameters, such as the pulse duration, intensity, and wavelength [22]. The criteria for observation of the SFPH have also been investigated over a broad range of the laser intensity and wavelength [23]. Ellipticity is another crucial parameter for the laser pulse. However, to the best of our knowledge, the dependence of the holographic pattern on the laser ellipticity has not been investigated before. In the elliptically polarized laser field, the rescattering electron travels along a two-dimensional trajectory in the laser polarization plane. This might make the SFPH in the elliptically polarized laser pulses more complex than that in linearly polarized laser fields.

To better understand the SFPH in elliptically polarized laser fields, we report on the scaling of the holographic pattern with the laser ellipticity in this Letter. We measure the PMDs from the ionization of Ar atoms in elliptically polarized laser pulses with the ellipticities ranging from 0 to 0.3 at the wavelength of 800 nm. We find that the spacing of the holographic fringe decreases gradually with increasing of the ellipticity. Based on the strong-field approximation (SFA) model, we show that the decrease of the holographic fringe spacing comes from the faster change of the phase difference between the direct and rescattering electrons due to the larger initial transverse momenta at larger ellipticities. With increasing of the laser ellipticity, a ridge structure appears in the low-energy region, which comes from forward scattering electrons. The critical conditions are obtained for the observation of the photoelectron holography and ridge structure in the elliptically polarized laser fields.

Experimentally, we used a cold target recoil ion momentum spectroscopy (COLTRIMS) to measure the PMDs of Ar atoms

exposed in strong laser pulses [24] (for the principle, see Ref. [25]). The laser pulses were generated from a Ti:sapphire femtosecond laser system with a repetition rate of 5 kHz at the center wavelength $\lambda$ of 800 nm. The pulse duration was almost 40 fs. The generated laser pulse was initially linearly polarized, and its polarization was controlled by a $\lambda/2$ plate and a $\lambda/4$ plate with rotating of the $\lambda/2$ plate. The laser pulse was then focused into the supersonic beam in the main chamber of the COLTRIMS system by a parabolic mirror ($f = 75$ mm). A uniformed electric field at about 8.5 V/cm and a uniformed magnetic field at about 8.7 G were used to collect the photoelectrons and photoions. The three-dimensional momenta of the electrons and ions were reconstructed from the time of flights and the positions of the particles on the detectors. The laser intensity in the experiment was almost $(1.3 \pm 0.2) \times 10^{14}$ W/cm$^2$.

Figures 1(a)–1(c) show the measured PMDs from the single ionization of Ar atoms by strong laser fields with different ellipticities ($\lambda = 800$ nm). The laser ellipticities for Figs. 1(a)–1(c) are 0, 0.1, and 0.2, respectively. All the PMDs reveal distinct spider-like interference patterns, as marked by the dashed lines in Figs. 1(a)–1(c). Those spider-like structures come from the holographic interferences between the direct and forward scattering trajectories [14,22]. In the linearly polarized laser field [Fig. 1(a)], the spider-like structure is symmetric with $p_x = 0$. As expected, with increasing of the laser ellipticity, the holographic structure becomes asymmetric and, the momentum spectra rotate clockwise under the influence of the long-range Coulomb potential [26], as shown in Figs. 1(b) and 1(c).

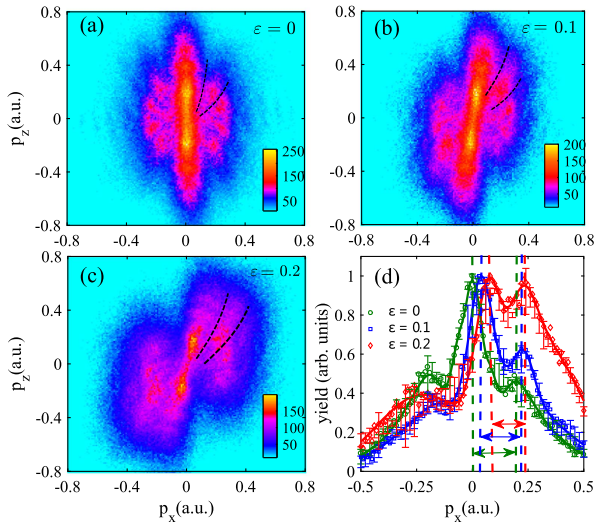


**Fig. 1.** (a)–(c) show the measured PMDs from single ionization of Ar in linearly and elliptically polarized laser pulses at the intensity of $1.3 \times 10^{14}$ W/cm$^2$ ($\lambda = 800$ nm) with the ellipticities of 0, ~0.1, and ~0.2, respectively. $p_z$ and $p_x$ are the electron momenta along the major and minor axes of the laser ellipse, respectively. The momentum spectra are integrated over $|p_y| < 0.05$ a.u., where $p_y$ is the momentum along the laser propagation direction. The dashed lines show the minima of the holographic patterns. (d) shows the measured momentum distributions along the $p_x$ direction at different ellipticities for $p_z = 0.3$ a.u. The slice range of $p_z$ is $0.3 \pm 0.01$ a.u. The vertical dashed lines and the arrows in (d) are used to show the fringe spacing of the holographic patterns.

To reveal how the holographic fringe scales with the laser ellipticity, we show in Fig. 1(d) a series of lineouts taken from Figs. 1(a)–1(c) at $p_z = 0.3$ a.u. for different ellipticities. One can see that the fringe spacing slightly changes with the laser ellipticity. To quantitatively show the scaling laws, we show in Fig. 2(a) the fringe spacing with respect to the ellipticity. One can see that the fringe spacing gradually decreases with the increase of the laser ellipticity at both $p_z = 0.3$ and $p_z = 0.2$ a.u.

In the following, we use a generalized strong-field approximation (gSFA) model to analyze the scaling of the photoelectron holographic pattern with the laser ellipticity, which has successfully predicted the scaling of the holographic fringe spacing with the laser intensity and wavelength [22]. The final electron momentum distribution within the gSFA is expressed as $\psi_{\text{total}} = \psi_{\text{sig}} + \psi_{\text{ref}}$, where $\psi_{\text{sig}}$ and $\psi_{\text{ref}}$ indicate the ionization probabilities of the rescattering electron (signal wave) and direct electron (reference wave), respectively. The phase of each trajectory is given by the classical action along the path, i.e., $S = -\int_{t_0}^{\infty}(v^2(t)/2 + I_p)\mathrm{d}t$. Therefore, the phase difference between the forward scattering and direct trajectories is

$$\Delta S = -\frac{1}{2}\int_{t_0^{\text{sig}}}^{t_c}(v_z^2 + v_x^2)\mathrm{d}t + \frac{1}{2}\int_{t_0^{\text{ref}}}^{t_c}(v_z^2 + v_x^2)\mathrm{d}t + I_p(t_0^{\text{sig}} - t_0^{\text{ref}}) + \Delta S^{\text{Im}}, \quad (1)$$

where $t_0^{\text{sig}}$ and $t_0^{\text{ref}}$ are the ionization times for the rescattering and direct electrons, respectively. $I_p$ is the ionization potential, $t_c$ is the rescattering time, and $\Delta S^{\text{Im}}$ is the difference of the classical action in imaginary time. The time-dependent electron velocities along the major and minor axes of the laser ellipse can be expressed as $v_z = v_{z0} + A_z(t) - A_z(t_0)$ and $v_x = v_{x0} + A_x(t) - A_x(t_0)$, respectively. $A_z(t)$ and $A_x(t)$ are the vector potentials along the major and minor axes, respectively. $v_{z0}$ and $v_{x0}$ are the initial velocities at the tunnel exit.

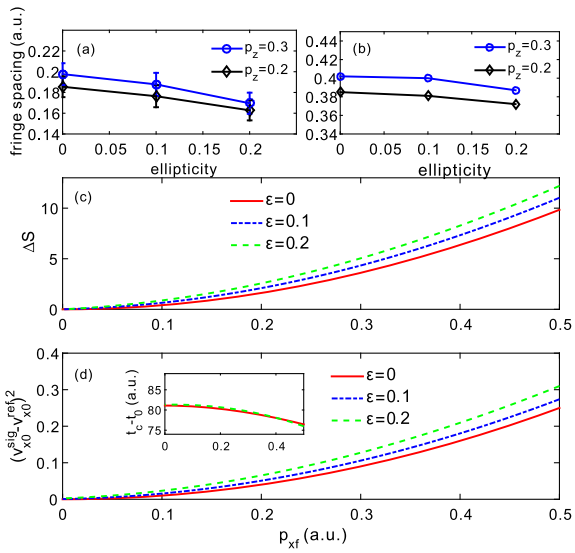


**Fig. 2.** (a) and (b) show the measured and simulated fringe spacing with respect to the laser ellipticity for $p_z = 0.3$ and $p_z = 0.2$ a.u. (c) and (d) show the calculated phase difference $\Delta S$ and $(v_{x0}^{\text{sig}} - v_{x0}^{\text{ref}})^2$ between the rescattering and direct trajectories with respect to $p_x$, respectively. The inset in (d) shows the time difference $(t_c - t_0)$ with respect to $p_x$.

The interference patterns are determined by this phase difference, i.e., $W = \cos^2(\Delta S/2)$. The ionization times and the initial velocities are obtained by solving the saddle-point equations. Here we have ignored the pre-exponential terms in the gSFA.

Figure 2(b) shows the fringe spacing of the holographic structure with respect to the ellipticity at $p_z = 0.3$ and $p_z = 0.2$ a.u. calculated by the gSFA model. One can see that the spacing of the holographic fringe calculated by the gSFA also decreases gradually with the laser ellipticity, which is consistent with the experimental results in Fig. 2(a). Comparing Fig. 2(a) with Fig. 2(b), one finds that the fringe spacing of the gSFA is larger than the experimental results, and the calculated shift in fringe spacing is smaller than those observed experimentally. This might be due to the effect of the Coulomb potential, which is neglected by the gSFA. It has been shown before that the long-range Coulomb potential has a significant influence on the SFPH [27]. As a result, the gSFA can only give qualitative agreement with the experiment [22].

We next analyze the scaling of the fringe spacing with the ellipticity by simplifying the phase difference in Eq. (1). The phase difference is simplified based on the following three assumptions: (1) the phase difference in imaginary time plays a minor role in the holographic pattern, (2) the interference pattern is mainly determined by the phase difference acquired in the $x$ axis, and (3) the ionization times of the direct and rescattering electrons are nearly the same, i.e., $t_0^{\mathrm{sig}} = t_0^{\mathrm{ref}} = t_0$. Thus, the phase difference in Eq. (1) can be expressed as

$$\Delta S \approx -(v_{x0}^{\mathrm{sig}} - v_{x0}^{\mathrm{ref}})^2 \cdot (t_c - t_0)/2. \tag{2}$$

In a linearly polarized laser field, Eq. (2) can be rewritten as $\Delta S = -p_x^2(t_c - t_0)/2$, because $v_{x0}^{\mathrm{sig}} = 0$ and $v_{x0}^{\mathrm{ref}} = p_x$. This phase difference has been identified as the key term responsible for the formation of the hologram in a linearly polarized laser field [14,22]. Figure 2(c) shows the phase difference calculated by Eq. (1) with respect to $p_x$ at $p_z = 0.3$ a.u. for three ellipticities. One can see that the phase difference $\Delta S$ increases faster with $p_x$ for larger ellipticities. According to Eq. (2), the holographic pattern (or the phase difference) scales with $(t_c - t_0)$ and $(v_{x0}^{\mathrm{sig}} - v_{x0}^{\mathrm{ref}})^2$. Figure 2(d) shows $(v_{x0}^{\mathrm{sig}} - v_{x0}^{\mathrm{ref}})^2$ with respect to $p_x$, and the inset of Fig. 2(d) shows the time difference $(t_c - t_0)$ with respect to $p_x$ for different ellipticities. One can see that $(t_c - t_0)$ is nearly the same for $\varepsilon = 0$ and 0.2, while the differences of the initial transverse momentum deviate with each other for different ellipticities. The dependence of $(v_{x0}^{\mathrm{sig}} - v_{x0}^{\mathrm{ref}})^2$ on $p_x$ [Fig. 2(d)] is very similar to the dependence of the phase difference on $p_x$ [Fig. 2(c)] for different ellipticities, which indicates that the assumptions 1, 2, and 3 are valid under our experimental condition. With increasing of the ellipticity, a larger initial transverse momentum for the rescattering electron is needed to counteract the electron motion along the minor axis of the laser ellipse. Because the phase difference between the rescattering and direct trajectories is proportional to $(v_{x0}^{\mathrm{sig}} - v_{x0}^{\mathrm{ref}})^2$, the phase difference will increase faster as a function of $p_x$. As a result, the fringe spacing becomes narrower with increasing of the ellipticity. Thus, the scaling of the fringe spacing with the ellipticity is mainly determined by the effect of the initial transverse momentum at the tunnel exit.

With increasing of the ellipticity to ~0.3, we see a clear ridge structure at almost $p_x = 0$ in Fig. 3(a), which is separated from the common two-lobe structure. This ridge structure has also been observed recently in elliptically polarized laser fields at a long wavelength of 3400 nm with small ellipticities of [0.07, 0.11] [28]. It was shown that the ridge structure comes from the forward scattering electrons, while the two-lobe structure comes from the direct electrons.

The question of the conditions under which the ridge structure appears in the PMD remains a key issue that should be addressed. We next investigate the critical ellipticities for the observation of the ridge structure in the elliptically polarized laser field. The ridge structure appears when two conditions are satisfied: (a) the direct electron and the rescattering electron are separated from each other in the PMD; and (b) the ionization probability of the rescattering electron is comparable to that of the direct electron. The conditions of (a) and (b), respectively, give the lower and upper limits for the ellipticities to observe the ridge structures.

According to condition (a), the ridge structure appears when the difference of the final momenta between the direct and forward scattering electrons is larger than the width of the PMD. The direct electron achieves a drift momentum $p_{\mathrm{drift}} = \varepsilon E_0/\omega$ from the laser field along the minor axis while the rescattering electrons mainly appear at almost $p_x = 0$. According to Delone–Krainov theory [29], the transverse momentum spread is a Gaussian distribution with a width of $\sigma_\perp = \sqrt{E_0/\sqrt{2I_p}}$. Thus, the critical condition to separate the direct and rescattering electrons in the PMD is $p_{\mathrm{drift}} = \sigma_\perp$. As a result, the lower limit of the ellipticity to observe the ridge structure is

$$\varepsilon = \frac{2\pi c}{\lambda}\sqrt{\frac{1}{E_0\sqrt{2I_p}}}, \tag{3}$$

where $c$ is the light speed.

According to condition (b), the ridge structure disappears when the ionization probability of the rescattering electron is much lower than that of the direct electron. The initial transverse momentum of the rescattering electron is $v_{x0}^{\mathrm{sig}} = \varepsilon E_0/\omega$ [30]. For a Gaussian distribution, the probability of the rescattering electron decreases to 0.01 of the maximal probability when $v_\perp = \sqrt{2\ln 10}\sigma_\perp$. Experimentally, it is difficult to observe the contribution of the rescattering electron with such

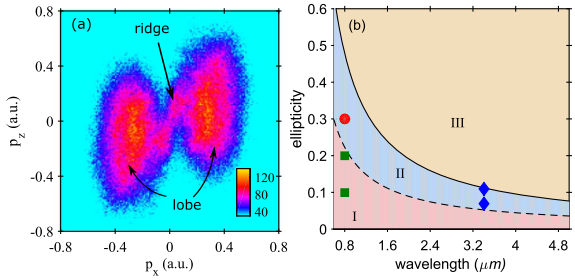


**Fig. 3.** (a) Measured PMD of Ar at the ellipticities of ~0.3. The same conditions are used as in Figs. 1(a)–1(c). (b) shows the phase diagram (laser ellipticity with respect to wavelength) for the holographic patterns and ridge structures in elliptically polarized laser pulses. The dashed and solid lines are the demarcation lines according to Eqs. (3) and (4), respectively. Three regions labeled I, II, and III are dissected by those two lines (see text for details). The squares and circles are the experimental data of this Letter, and the blue diamonds are the experimental data in Ref. [28].

low probability. Thus, the upper limit of the ellipticity to observe the ridge structure is $v_{x0}^{\mathrm{sig}} = \sqrt{2\ln 10}\sigma_{\perp}$, i.e.,

$$\varepsilon = \sqrt{2\ln 10}\frac{2\pi c}{\lambda}\sqrt{\frac{1}{E_0\sqrt{2I_p}}} \quad (4)$$

Because the critical ellipticities in Eqs. (3) and (4) are weakly dependent on the laser intensity and the ionization potential, in Fig. 3(b), we show the phase diagram (the ellipticity with respect to the wavelength) for the observation of the holographic pattern and ridge structure in elliptically polarized laser pulses. The dashed and solid lines are plotted according to Eqs. (3) and (4), respectively. The holographic pattern appears in region I, the ridge structure appears in region II, and neither of them appears in region III. When considering the Coulomb focusing effect, those two demarcation lines might be slightly shifted.

To validate the results in Eqs. (3) and (4), we show the experimental data of this Letter ($\lambda = 800$ nm) in Fig. 3(b). The holographic patterns appear at the ellipticities of 0.1 and 0.2 (green squares), and the ridge structure appears at 0.3 (red dot). These predictions agree well with the experimental results, as shown in Figs. 1 and 3(a). The blue diamonds in the region II of Fig. 3(b) show the experimental results in Ref. [28], where the ridge structure was observed at the ellipticities of 0.07 and 0.11 for the wavelength of 3400 nm. As expected, these two ellipticities are located in the region II of Fig. 3(b).

In summary, we measured the PMDs from single ionization of atoms in linearly and elliptically polarized laser pulses. We investigated the scaling of the photoelectron holography with the laser ellipticity for small ellipticities. We found that the spacing of the holographic fringe becomes gradually narrower with increasing of the ellipticity. The physical origin of the scaling of the photoelectron holography with the ellipticity is different from the scaling with other laser parameters, e.g., wavelength and intensity, in a linearly polarized laser field, where the time difference between the rescattering and ionization plays the crucial role [22]. In elliptically polarized laser fields, the initial transverse momenta become larger for larger ellipticity, leading to faster changes of the phase difference between the direct and forward scattering trajectories as a function of the final transverse momenta. With increasing of the laser ellipticity, the forward scattering electrons are separated from the direct electrons in the PMD, forming a ridge structure in the low-energy region. We have obtained the critical condition to observe the photoelectron holography and ridge structure in the PMDs, shedding light on the rescattering effect in elliptically polarized laser fields. The separation of the direct and forward scattering electron in the PMD is potentially valuable and may open a new door towards probing molecular structure and dynamics using the forward scattering electrons [31].

**Funding.** National Natural Science Foundation of China (NSFC) (11627809, 11674116, 11722432); Program for HUST Academic Frontier Youth Team.

## REFERENCES

1. P. B. Corkum, Phys. Rev. Lett. **71**, 1994 (1993).
2. J. L. Krause, K. J. Schafer, and K. C. Kulander, Phys. Rev. Lett. **68**, 3535 (1992).
3. L. Li, P. Lan, L. He, X. Zhu, J. Chen, and P. Lu, Phys. Rev. Lett. **120**, 223203 (2018).
4. H. Yuan, L. He, F. Wang, B. Wang, X. Zhu, P. Lan, and P. Lu, Opt. Lett. **43**, 931 (2018).
5. B. Wang, L. He, F. Wang, H. Yuan, X. Zhu, P. Lan, and P. Lu, Phys. Rev. A **97**, 013417 (2018).
6. C. Zhai, X. Zhang, X. Zhu, L. He, Y. Zhang, B. Wang, Q. Zhang, P. Lan, and P. Lu, Opt. Express **26**, 2775 (2018).
7. L. He, Q. Zhang, P. Lan, W. Cao, X. Zhu, C. Zhai, F. Wang, W. Shi, M. Li, X. Bian, P. Lu, and A. D. Bandrauk, Nat. Commun. **9**, 1108 (2018).
8. D. N. Fittinghoff, P. R. Bolton, B. Chang, and K. C. Kulander, Phys. Rev. Lett. **69**, 2642 (1992).
9. B. Walker, B. Sheehy, L. F. DiMauro, P. Agostini, K. J. Schafer, and K. C. Kulander, Phys. Rev. Lett. **73**, 1227 (1994).
10. Y. Chen, Y. Zhou, Y. Li, M. Li, P. Lan, and P. Lu, Phys. Rev. A **97**, 013428 (2018).
11. S. Luo, X. Ma, H. Xie, M. Li, Y. Zhou, W. Cao, and P. Lu, Opt. Express **26**, 13666 (2018).
12. M. Meckel, D. Comtois, D. Zeidler, A. Staudte, D. Pavicic, H. C. Bandulet, H. Pépin, J. C. Kieffer, R. Dörner, D. M. Villeneuve, and P. B. Corkum, Science **320**, 1478 (2008).
13. C. I. Blaga, J. Xu, A. D. DiChiara, E. Sistrunk, K. Zhang, P. Agostini, T. A. Miller, L. F. DiMauro, and C. D. Lin, Nature **483**, 194 (2012).
14. Y. Huismans, A. Rouzée, A. Gijsbertsen, J. Jungmann, A. Smolkowska, P. Logman, F. Lépine, C. Cauchy, S. Zamith, T. Marchenko, J. Bakker, G. Berden, B. Redlich, A. van der Meer, H. Muller, W. Vermin, K. J. Schafer, M. Spanner, M. Yu. Ivanov, O. Smirnova, D. Bauer, S. V. Popruzhenko, and M. J. J. Vrakking, Science **331**, 61 (2011).
15. X.-B. Bian and A. D. Bandrauk, Phys. Rev. Lett. **108**, 263003 (2012).
16. M. Haertelt, X.-B. Bian, M. Spanner, A. Staudte, and P. B. Corkum, Phys. Rev. Lett. **116**, 133001 (2016).
17. M. Meckel, A. Staudte, S. Patchkovskii, D. M. Villeneuve, P. B. Corkum, R. Dörner, and M. Spanner, Nat. Phys. **10**, 594 (2014).
18. M.-M. Liu, M. Li, C. Wu, Q. Gong, A. Staudte, and Y. Liu, Phys. Rev. Lett. **116**, 163004 (2016).
19. Y. Zhou, O. I. Tolstikhin, and T. Morishita, Phys. Rev. Lett. **116**, 173001 (2016).
20. M. He, Y. Li, Y. Zhou, M. Li, W. Cao, and P. Lu, Phys. Rev. Lett. **120**, 133204 (2018).
21. S. G. Walt, N. B. Ram, M. Atala, N. Shvetsov-Shilovski, A. von Conta, D. Baykusheva, M. Lein, and H. Wörner, Nat. Commun. **8**, 15651 (2017).
22. Y. Huismans, A. Gijsbertsen, A. S. Smolkowska, J. H. Jungmann, A. Rouzée, P. S. W. M. Logman, F. Lépine, C. Cauchy, S. Zamith, T. Marchenko, J. M. Bakker, G. Berden, B. Redlich, A. F. G. van der Meer, M. Yu. Ivanov, T.-M. Yan, D. Bauer, O. Smirnova, and M. J. J. Vrakking, Phys. Rev. Lett. **109**, 013002 (2012).
23. T. Marchenko, Y. Huismans, K. J. Schafer, and M. J. J. Vrakking, Phys. Rev. A **84**, 053427 (2011).
24. H. Xie, M. Li, S. Luo, Y. Li, Y. Zhou, W. Cao, and P. Lu, Phys. Rev. A **96**, 063421 (2017).
25. J. Ullrich, R. Moshammer, A. Dorn, R. Dörner, L. Ph. H. Schmidt, and H. Schmidt-Böcking, Rep. Prog. Phys. **66**, 1463 (2003).
26. S. P. Goreslavski, G. G. Paulus, S. V. Popruzhenko, and N. I. Shvetsov-Shilovski, Phys. Rev. Lett. **93**, 233002 (2004).
27. W. Yang, H. Zhang, C. Lin, J. Xu, Z. Sheng, X. Song, S. Hu, and J. Chen, Phys. Rev. A **94**, 043419 (2016).
28. J. Maurer, B. Willenberg, J. Daněk, B. W. Mayer, C. R. Phillips, L. Gallmann, M. Klaiber, K. Z. Hatsagortsyan, C. H. Keitel, and U. Keller, Phys. Rev. A **97**, 013404 (2018).
29. N. B. Delone and V. P. Krainov, J. Opt. Soc. Am. B **8**, 1207 (1991).
30. M. Li, L. Qin, C. Wu, L.-Y. Peng, Q. Gong, and Y. Liu, Phys. Rev. A **89**, 013422 (2014).
31. W. Yang, Z. Sheng, X. Feng, M. Wu, Z. Chen, and X. Song, Opt. Express **22**, 2519 (2014).